

# Plasmons Enhancing Sub-Bandgap Photoconductivity in TiO<sub>2</sub> Nanoparticles Film

Mohammed A. Ibrahim,\* Emanuele Verrelli, Ali M. Adawi,\* Jean-Sebastien G. Bouillard,\* and Mary O'Neill\*



Cite This: *ACS Omega* 2024, 9, 10169–10176



Read Online

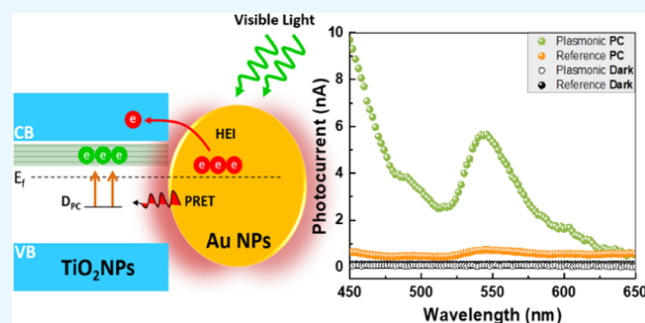
ACCESS |

Metrics & More

Article Recommendations

Supporting Information

**ABSTRACT:** The coupling between sub-bandgap defect states and surface plasmon resonances in Au nanoparticles and its effects on the photoconductivity performance of TiO<sub>2</sub> are investigated in both the ultraviolet (UV) and visible spectrum. Incorporating a 2 nm gold nanoparticle layer in the photodetector device architecture creates additional trapping pathways, resulting in a faster current decay under UV illumination and a significant enhancement in the visible photocurrent of TiO<sub>2</sub>, with an 8-fold enhancement of the defects-related photocurrent. We show that hot electron injection (HEI) and plasmonic resonance energy transfer (PRET) jointly contribute to the observed photoconductivity enhancement. In addition to shedding light on the below-band-edge photoconductivity of TiO<sub>2</sub>, our work provides insight into new methods to probe and examine the surface defects of metal oxide semiconductors using plasmonic resonances.



## 1. INTRODUCTION

Due to their potential for clean and sustainable technology, light harvesting materials and strategies have gained considerable attention in the last couple of years. TiO<sub>2</sub> is extensively investigated due to its direct wide bandgap and tunable electrical and optical properties that originate from its intragap energy levels related to inherited surface defects and oxygen vacancies.<sup>1,2</sup> Such unique properties enable TiO<sub>2</sub> to be highly desirable in light harvesting applications such as photocatalysis,<sup>3</sup> photovoltaics,<sup>4</sup> photodetection,<sup>5</sup> and photoelectrochemical sensing.<sup>6</sup> Due to its hypotoxicity and abundance, developing efficient photoconductivity of TiO<sub>2</sub> in the visible band will significantly impact the environment and device production cost.<sup>7</sup> Several attempts to extend the optical absorption of TiO<sub>2</sub> to the visible spectral region by doping with different materials have been reported.<sup>3,8–10</sup> In parallel, reducing the bandgap of TiO<sub>2</sub> by defects engineering has also been considered by deliberately introducing Ti<sup>3+</sup>, lattice disorder defects, and oxygen defects within the crystalline structure of TiO<sub>2</sub>.<sup>11–13</sup> However, these attempts often lack long-term stability and repeatability.<sup>14</sup>

As an attractive alternative, the strong field enhancement and confinement of localized surface plasmon resonances (LSPR) represent an efficient strategy to stimulate visible photoresponses in many metal oxide semiconductors. Possible mechanisms are plasmonic energy conversion by hot electron injection (HEI) to a nearby semiconductor<sup>15,16</sup> and near-field coupling and energy transfer, sometimes called plasmonic

resonance energy transfer (PRET).<sup>17</sup> Near-field coupling, or PRET, requires spectral overlap between the semiconductor absorption and the LSPR, whereas HEI relies on the injection of hot charge carriers from the plasmon decay through the Schottky barrier.<sup>6,18,19</sup>

TiO<sub>2</sub>-based hybrid systems have been widely studied to enhance and extend the optoelectronic response of TiO<sub>2</sub> into the visible and near-IR, enabling a wide range of applications from photocatalysis to sensing and photodetectors.<sup>6,8,16,20–28</sup> Shu et al.<sup>6</sup> investigated the coupling interaction of surface defects engineered in TiO<sub>2</sub> nanobars with the plasmonic field of gold nanoparticles (Au NPs) in the UV and visible for photoelectrochemical biosensing applications. Their results show a 25% reduction in UV response combined with a 6- to 7-fold increase in the visible photoconductivity, in the presence of Au NPs. Chen et al.<sup>20</sup> reported visible surface defect photocurrent enhancement in TiO<sub>2</sub>:Au nanocomposite film due to electron–hole pairs generated via PRET and HEI. Tan et al.<sup>29</sup> extended this to the near-IR using a TiO<sub>2</sub>–Au bilayer. Naldoni et al.<sup>30</sup> observed a similar behavior by introducing oxygen defect states via doping of the TiO<sub>2</sub> and highlighted the

**Received:** September 11, 2023

**Revised:** January 16, 2024

**Accepted:** January 24, 2024

**Published:** February 20, 2024



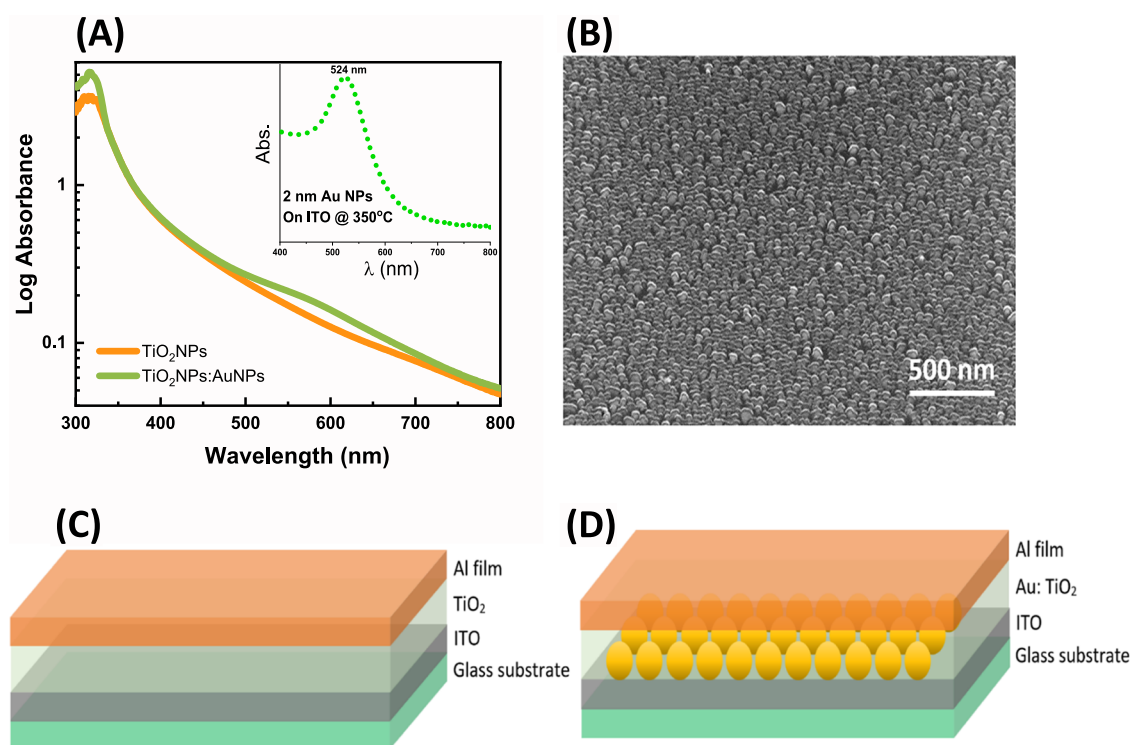


**Figure 1.** (A) Semilog plot of the absorption spectra of TiO<sub>2</sub> NPs films with and without Au NPs. The inset shows the absorption spectrum of ITO \ Au NPs after annealing for 1 h at 350 °C in air (shown in (B)). (B) SEM image of Au NPs film on ITO substrate after annealing at 350 °C for 1 h in air. (C, D) Structures and configuration of the metal–semiconductor–metal devices utilized in this work, the reference device with no Au NPs and the plasmonic device with Au NPs layer, respectively.

importance of both the interband transitions and the plasmonic resonance in TiO<sub>2</sub>:Au systems.

In this work, we report on unusually spectrally narrow defects photocurrent in the visible region in a vertical metal–semiconductor–metal (MSM) device configuration, with a full width at half-maximum (fwhm) under 40 nm obtained for illumination at a wavelength of  $\sim$ 545 nm. Unlike conventional charge collection devices, our device structure shows a defined defect-based visible photocurrent under zero bias, with the visible photocurrent showing an 8-fold enhancement when decorated with thermally evaporated Au nanoparticles. This significant enhancement in photocurrent is attributed to the combined effect of HEI and near-field/PRET processes stimulated by the plasmonic resonance of the Au nanostructures interfaced with TiO<sub>2</sub>. Our findings can assist the study of localized surface defects in wide-bandgap semiconductors; they also represent a strategy to enhance the selective photocatalytic reaction of TiO<sub>2</sub> and develop an advanced photoelectric material for biosensing applications.

## 2. RESULTS AND DISCUSSION

Figure 1A shows the optical absorption spectra of TiO<sub>2</sub> nanoparticle (TiO<sub>2</sub> NP) films with and without the Au NPs layer. The absorption peak around a wavelength of 322 nm (3.8 eV) corresponds to the fundamental band-to-band electronic transition. This absorption peak occurs at a higher energy than the expected transition energy of TiO<sub>2</sub> (3.2 eV) and can be attributed to the quantum confinement effect of the TiO<sub>2</sub> nanoparticles.<sup>31</sup> The plot also shows a long absorption tail that decays into the visible spectrum region, attributed to surface defects.<sup>20,32</sup> The visible absorption is further increased after the incorporation of Au nanoparticles due to the

plasmonic resonance effect. This plasmonic absorption peak is red-shifted compared to the Au nanoparticles absorption on ITO in air (before the deposition of TiO<sub>2</sub> NPs film shown in the inset of Figure 1A) due to the higher refractive index of the TiO<sub>2</sub> nanoparticles film now surrounding the Au NPs.

The photoconductivity of both the reference and the plasmonic devices shows the characteristic UV response of the TiO<sub>2</sub> nanoparticle films, arising from the direct band-to-band electron transitions and the visible band arising from defect states.<sup>5,33</sup> Figure 2 shows the photoconductivity

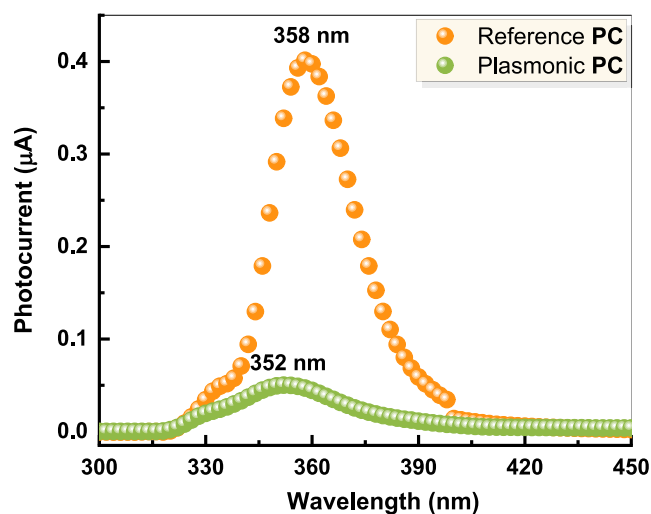


**Figure 2.** Photocurrent spectra of the reference and the plasmonic devices at 0 V bias showing the photocurrent scanning range from 300–450 nm.

spectrum of each device at 0 V bias over the spectral range of 300 to 450 nm. Both devices show photoconductivity in the UV, reaching a photocurrent of 0.4 and 0.054  $\mu\text{A}$  for the reference and plasmonic devices, respectively. The drop in UV photocurrent in the presence of gold nanoparticles is associated with additional charge trapping at the metal–semiconductor interface and electron trapping from the  $\text{TiO}_2$  to the Au NPs.<sup>20,34</sup> In parallel, the addition of the Au NPs causes band bending and charge trapping at the  $\text{TiO}_2$ –Au interface,<sup>35,36</sup> resulting in the observed blue shift in the UV photocurrent from 358 to 352 nm, with corresponding increased fwhm from 27.4 to 36.3 nm (Figure 2).

In addition to the UV response observed in Figure 2, a clear photocurrent enhancement in the visible range (450–650 nm) can be observed (Figure 3A). This photocurrent increases at energies well below the  $\text{TiO}_2$  bandgap and can be linked to HEI, where the plasmon decay results in hot electrons with sufficient energy to overcome the Schottky barrier. This is illustrated by the calculated Fowler function for a gold– $\text{TiO}_2$  interface<sup>37–42</sup> (Figure 3A).

Additionally, both devices show a pronounced photocurrent peak around 545 nm (inset of Figure 3A), corresponding to the transition between the surface defect and the conduction band in  $\text{TiO}_2$ ,<sup>43</sup> with a photoconductivity 8 times larger in the plasmonic device than the reference device. This can be attributed to the dipole interaction between surface plasmons and sub-bandgap energy states of surface defects through the PRET process, where the strong plasmonic near-field enhancement of Au NPs leads to an efficient transition between the surface defect and the conduction band in  $\text{TiO}_2$ . Another photocurrent peak evolved at higher photon energy, below the plasmonic resonance of Au NPs (458 nm), and corresponds to light absorption in gold due to electronic transitions from the d-bands to the sp-bands.<sup>44,45</sup> The photocurrent enhancement at this shorter wavelength is mainly related to the optical absorption of  $\text{TiO}_2$  NPs and scattering by the Au NPs. This is further supported by the spectral overlap between the incident photon-to-electron conversion efficiency (IPCE) of the plasmonic device and the absorption spectrum of the gold nanoparticles inside the device, normalized to the reference device to remove the  $\text{TiO}_2$  component shown in Figure 3B.

To probe the photocurrent dynamics, the temporal response of the reference and the plasmonic devices were recorded at 0 V under both UV ( $355 \pm 5$  nm) and visible ( $545 \pm 5$  nm) irradiation, in 1 min on/off cycles as shown in Figure 4A,B. Both devices show a fast rise and decay in photocurrent when UV irradiation is switched on and off, with an order of magnitude higher photocurrent from the reference device than the plasmonic one (Figure 4A). The rise and decay time constants were measured to be  $\tau_r = 5.9$  s and  $\tau_d = 6$  s, respectively, for the reference device, and  $\tau_r = 4.4$  s and  $\tau_d = 3.8$  s for the plasmonic device. Table 1 provides a comparison of the UV temporal responses of  $\text{TiO}_2$ -based photodetector devices and our work.

The reference device shows a slow exponential-like decay of the photocurrent even when illumination is maintained (Figure 4A). This reduction in photocurrent during illumination is attributed to charge trapping of the charge carriers on the surface of  $\text{TiO}_2$  after excitation.<sup>58,59</sup> In addition, the peak photocurrent in the reference device decreases with each illumination cycle, highlighting long-lived processes, potentially arising from charge accumulation in trap states, impeding the charge carrier flow in the device. On the other hand, the

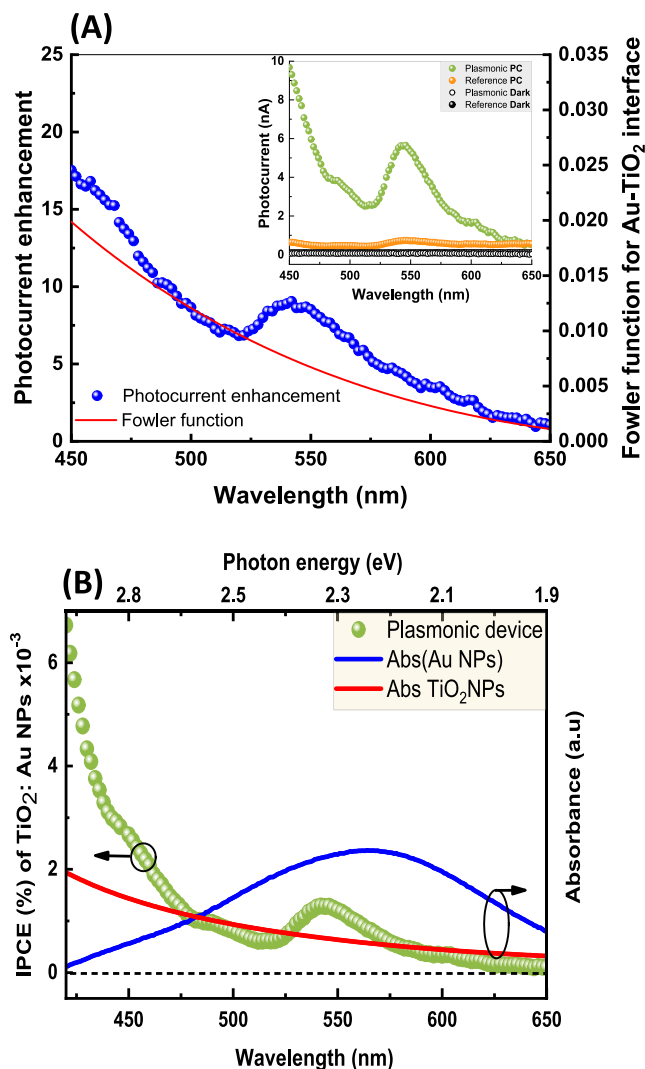


**Figure 3.** (A) Photocurrent enhancement spectrum (normalized to the reference device) of the plasmonic device at 0 V bias with the Fowler function for a gold– $\text{TiO}_2$  interface. The inset shows the photocurrent spectra of the reference and the plasmonic devices at 0 V bias (normalized to the light spectrum intensity), along with the dark current for each device. (B) IPCE of the  $\text{TiO}_2$  NPs-incorporated Au NPs showing the spectral absorption overlap between defects-related absorption spectrum (red curve) and the plasmonic absorption of Au NPs (blue curve) acquired by subtracting the absorption of  $\text{TiO}_2$  NPs film from the absorption of  $\text{TiO}_2$  NPs + Au NPs film shown in Figure 1A.

plasmonic device shows a spike-like photocurrent signal followed by a significantly lower but stable photocurrent. The incorporation of Au NPs in the plasmonic device creates additional effective trapping pathways, such as interfacial sites at the  $\text{TiO}_2$ –Au,<sup>35</sup> leading to a faster decay in the UV photocurrent, overcoming the long-lived trap states, resulting in the observed photocurrent (Figure 4A).

Figure 4B shows the temporal responses of the reference and plasmonic devices upon visible illumination. The incorporation of Au NPs has significantly enhanced the sub-bandgap photoconductivity compared to the reference device (with no Au NPs) due to the effect of the plasmonic resonance excitation of electrons in the Au NPs. The corresponding time constants were measured as  $\tau_r = 2.5$  s and  $\tau_d = 5$  s for the reference device, and  $\tau_r = 5.6$  s and  $\tau_d = 4.5$  s for the plasmonic

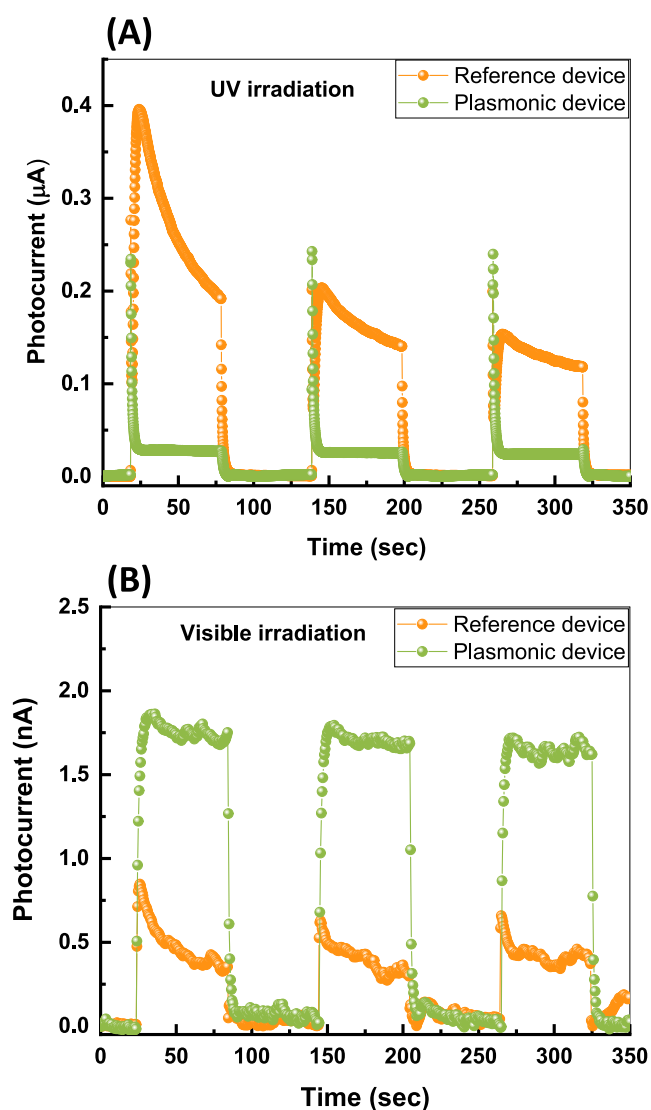


**Figure 4.** Photocurrent of the reference and the plasmonic devices as a function of time at 0 V bias in response to a 1 min incident light pulse at (A) UV and (B) visible.

device. This temporal response of the plasmonic device is comparable to recently reported time responses for  $\text{TiO}_2/\text{Au}$  NPs<sup>60,61</sup> and slower than the self-powered heterojunction device based on  $\text{CuI}/\text{TiO}_2$ <sup>62</sup> and could be used for UV switching applications with frequencies of a few hertz.

The principal mechanism by which photogenerated charge carriers move in our plasmonic device differs from that of conventional charge collection devices working with external bias. In such devices, electrons and holes move in opposite directions, following the electric field provided by the external source. Furthermore, the photoresponse time will highly depend on environmental conditions, such as the oxygen adsorption/desorption process, which often leads to long photoresponse times.<sup>1</sup> On the contrary, in our plasmonic device, charge carriers are separated and driven in opposite directions by the built-in photovoltaic field stimulated from the Schottky junction established at the interface between Au NPs and  $\text{TiO}_2$  nanoparticles film. This enables the plasmonic device to have a fast photoresponse without needing an external field source.<sup>50</sup>

A physical picture showing the working mechanism of the devices with and without the incorporation of Au NPs upon UV and visible light irradiation is schematically illustrated in Figure 5. In the reference device, UV photocurrent corresponds to the standard transition from the valence band to the conduction band, whereas the visible photocurrent arises from the excitation of electrons from sub-bandgap energy states into the conduction band of the  $\text{TiO}_2$  (Figure 5A,B). The Schottky junction between the ITO (work function: 4.7 eV) and the  $\text{TiO}_2$  NPs (conduction band edge: 4.2 eV)<sup>63</sup> with a junction height estimated to be 0.5 eV is the main driving force of the photo charge carriers' dissociation, which powers the device without needing an external field.

However, in the plasmonic device, the Schottky junction between the Au NPs (work function: 5.1 eV) and the  $\text{TiO}_2$  NPs with an overall junction height of about 0.9 eV (according to band alignment) creates the internal electric field, forcing the photogenerated electrons and holes to move in opposite directions.<sup>64</sup> The smaller Schottky height in the reference device explains the higher UV photocurrent than that in the plasmonic device. The existence of Au NPs can also trap the photo charge carriers by acting as a charge sink due to a work function difference, which will further reduce the UV photocurrent in the plasmonic device.<sup>30,35</sup> Due to the relatively small difference in work function between the  $\text{TiO}_2$  and the aluminum (Al) back electrode (4.3 eV),<sup>54,55</sup> the junction can be treated as an ohmic contact.

In the case of visible light irradiation, on the other hand, electrons trapped at the surface defects will be excited to the conduction band leading to sub-bandgap photoactivity. The observed 8-fold enhancement in visible photoconductivity in the plasmonic device is attributed to the coupling between the sub-bandgap defect states and the surface plasmons of Au nanoparticles. Two plasmonic mechanisms are jointly responsible for the sub-bandgap photocurrent enhancement in  $\text{TiO}_2$  in the plasmonic device: hot electrons injection (HEI) and plasmonic resonance energy transfer (PRET), illustrated in Figure 5C. These plasmonic mechanisms mainly enhance the photoconductivity in semiconductor devices,<sup>6,56,57</sup> despite the higher Schottky barrier; however, their active engagement with the sub-bandgap defect states is not yet considered widely in the literature.

### 3. CONCLUSIONS

In summary, a spectrally narrow photoresponse in the visible region was observed from a 20 nm  $\text{TiO}_2$  NPs (P25) layer in a vertical configuration metal–semiconductor–metal device at 0 applied voltage. This significant sub-bandgap photocurrent is attributed to the inherited surface defects and liberation of trapped electrons to the conduction band. Defect electron transition is found to be enhanced significantly after the incorporation of Au nanoparticles. HEI and PRET are jointly responsible for this enhancement due to the direct contact between Au nanoparticles and  $\text{TiO}_2$  nanoparticles film and the excellent overlap between the plasmonic resonance of the Au NPs and the absorption spectrum of the surface defects of the  $\text{TiO}_2$  nanoparticles film. This study outlines the active interaction between surface defects and surface plasmons, which could be highly beneficial in studying surface defects in semiconductors. A physical model explaining charge injection and separation based on HEI and PRET is proposed. Our findings could be of interest in imaging applications where a solution-processed  $\text{TiO}_2$  photodetector, with different photo-

Table 1. Comparison of the Temporal Responses of Our Work and Those of Previous Reports

| photodetector                     | bias (V) | UV photoresponse |              |              | visible/NIR photoresponse |   |  | refs |
|-----------------------------------|----------|------------------|--------------|--------------|---------------------------|---|--|------|
|                                   |          | $\lambda$ (nm)   | $\tau_r$ (s) | $\tau_d$ (s) | $\lambda$ (nm)            | $\tau_r$ (s)                              | $\tau_d$ (s)                             |      |
| TiO <sub>2</sub> film             | 5        | 365              | 0.017        | 0.019        |                           |   |  | 46   |
| TiO <sub>2</sub> NTs/Ag NPs       | 1        | 365              | 0.43         | 0.70         |                           |   |  | 47   |
| TiO <sub>2</sub> NRs/Ag NPs       | 1        | 365              | 3.90         | 5.70         |                           |   |  | 47   |
| TiO <sub>2</sub> /Ag porous films | 0        | 450              | 112 $\mu$ s  | 24 $\mu$ s   | 660                       |   |  | 48   |
| TiO <sub>2</sub> NWs/Ag NPs       | 3        | 350              | 0.56         | 0.13         | white light               | 0.24                                      | 0.14                                     | 49   |
| TiO <sub>2-x</sub> /Au NPs        |          | 365              |              |              | 450,520, 585, 630         |   |  | 6    |
| TiO <sub>2</sub> /spiro-MeOTAD    | 0        |                  |              |              | 410                       | 0.12                                      | 0.06                                     | 50   |
| Au/TiO <sub>2</sub> /NR/Au        | -4       | 350              |              |              | 400,470,570               |   |  | 51   |
| ZnO NPs                           | 20       | 363              | >0.5         |              | 545                       | 6.5                                       | $\tau_{d1} = 2.5$<br>$\tau_{d2} = 18.8$  | 1    |
|                                   |          |                  |              |              | 596                       | 14.5                                      | $\tau_{d1} = 6.6$<br>$\tau_{d2} = 25.6$  |      |
| ZnO NPs/Au                        | 0.01     | 363              |              |              | 850                       | $\tau_{r1} = 9.5$<br>$\tau_{r2} = 73.5$   | $\tau_{d1} = 15.5$<br>$\tau_{d2} = 81.7$ | 16   |
| ZnO NWs/Au NRs                    |          |                  |              |              | 650                       | $\tau_{r1} = 6.3$<br>$\tau_{r2} = 0.238$  | $\tau_{d1} = 16.5$<br>$\tau_{d2} = 0.69$ | 52   |
|                                   |          |                  |              |              | 850                       |   |  |      |
| MoS <sub>2</sub> /Au              |          |                  |              |              | 532                       | $\tau_{r1} = 28.5$<br>$\tau_{r2} = 494.3$ | 232                                      | 53   |
|                                   |          |                  |              |              | 1070                      | $\tau_{r1} = 44.5$<br>$\tau_{r2} = 404.7$ | 216.5                                    |      |
| this work                         | 0        | 355              | 4.4          | 3.8          | 545                       | 5.6                                       | 4.5                                      |      |

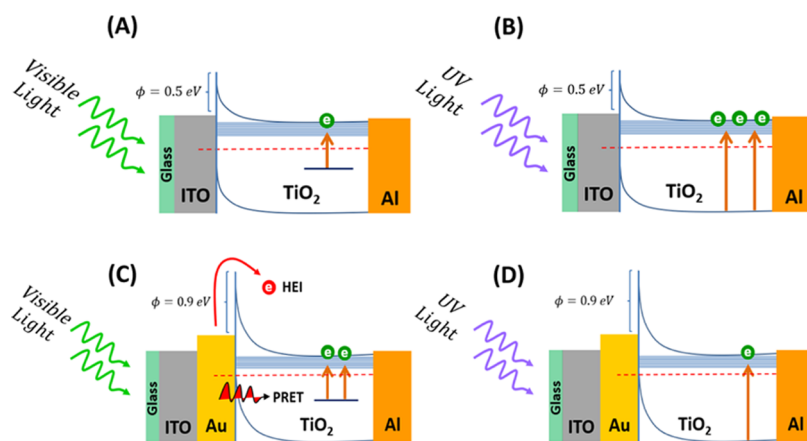


**Figure 5.** Schematic energy band diagrams illustrating the photoconductivity mechanisms for the reference device upon light irradiation in the (A) visible and (B) UV regions, and the plasmonic device upon light irradiation in the (C) visible and (D) UV regions. Hot electron injection (HEI) and plasmonic resonance energy transfer (PRET) are responsible for the visible photocurrent enhancement after the incorporation of Au nanoparticles in the plasmonic device.

responses, UV and visible, is possible. It also benefits those who are investigating selective photocatalytic reactions based on TiO<sub>2</sub>.

#### 4. EXPERIMENTAL SECTION

Two different devices with vertical configuration structures, a reference device (ITO/TiO<sub>2</sub>NPs/Al) and a plasmonic device (ITO/Au/TiO<sub>2</sub>NPs/Al), were considered (Figure 1C,D). Devices were fabricated on a float glass substrate with prepatterned interdigitated indium tin oxide (ITO) electrodes (20  $\Omega$ /square) with overall channel dimensions (device area) of 3 mm  $\times$  1.5 mm, (Ossila Ltd.). ITO substrates were thoroughly cleaned using an ultrasonic bath in three consecutive solutions, acetone, ethanol, and distilled water, and then dried with N<sub>2</sub>. The substrates were then treated with UV/ozone for 3 min to remove any organic contaminants and

impurities remaining on the surface and improve surface wettability.

The plasmonic device was fabricated by thermally evaporating Au directly on the ITO substrate with a deposition rate of 0.1  $\text{\AA}/\text{s}$  at  $5 \times 10^{-7}$  mbar using an HHV Auto 500 multifunctional automated evaporator, resulting in a nominal thickness of 2 nm. The sample was then annealed in air at 350  $^{\circ}\text{C}$  for 1 h, leading to the dewetting of the Au layer, resulting in a dense layer of Au nanoparticles with  $45 \pm 5$  nm diameter distributed uniformly over the substrate (Figure 1B).

For both the plasmonic and reference devices, TiO<sub>2</sub> nanoparticles suspension of concentration 10% by weight in deionized water was prepared using commercial TiO<sub>2</sub> NPs powder (P25) with a particle diameter of 20 nm bought from Sigma-Aldrich, containing a mix of rutile and anatase phases. Before deposition, the solution was filtered with a 0.45  $\mu\text{m}$

poly(tetrafluoroethylene) (PTFE) syringe filter to improve film quality.

The filtered suspension of TiO<sub>2</sub> NPs is then spin-cast on top of Au NPs at a speed of 2000 rpm for 30 s. These deposition conditions were optimized to obtain TiO<sub>2</sub> nanoparticle films of 200 nm thickness ( $\pm 5$  nm) measured using a Dektak profilometer from Bruker. The overall hybrid structure was baked in air at 150 °C for 10 min before a 150 nm aluminum (Al) film was thermally evaporated to form the device back electrode. A reference device was fabricated following the same fabrication procedure without incorporating the Au NPs layer. A thickness of 200 nm was used for the TiO<sub>2</sub> nanoparticle film in order to avoid short-circuiting the device when depositing the top electrode (Al) through this porous layer.

Optical absorption was measured before evaporating the back Al electrode using a Thermo Scientific (EVOLUTION 220) spectrophotometer over the 300 to 900 nm spectral range. *I*–*V* and photocurrent measurements were recorded using a xenon lamp with a 5 nm bandwidth monochromator and two electrical needle probes interfaced to a Keithley 2400 source meter using BenWin+ software to record the photocurrent as a function of wavelength and applied voltage. The light intensity was monitored using a digital compact power and energy meter console with calibrated photodiode sensors from Thorlabs (PM100D). Devices were irradiated at a normal incident angle through the glass/ITO side, with the light beam covering the whole device's active area. All of the measurements were done at room temperature in the air.

## ■ ASSOCIATED CONTENT

### SI Supporting Information

The Supporting Information is available free of charge at <https://pubs.acs.org/doi/10.1021/acsomega.3c06932>.

*I*–*V* curves of the photodetector devices under dark and visible irradiation, optical images of the photodetector device and Au NPs films, and explanation of Fowler function (PDF)

## ■ AUTHOR INFORMATION

### Corresponding Authors

**Mohammed A. Ibrahim** – *Laser Sciences and Technology Branch, Applied Sciences Department, University of Technology, Baghdad 10066, Iraq; UNAM-Institute of Materials Science and Nanotechnology and National Nanotechnology Research Center, Bilkent University, Ankara 06800, Turkey;* [orcid.org/0000-0003-4721-3815](https://orcid.org/0000-0003-4721-3815);  
Email: [mohammed.a.ibrahim@uotechnology.edu.iq](mailto:mohammed.a.ibrahim@uotechnology.edu.iq)

**Ali M. Adawi** – *Department of Physics and Mathematics, University of Hull, Kingston upon Hull HU6 7RX, United Kingdom;* [orcid.org/0000-0001-6850-5679](https://orcid.org/0000-0001-6850-5679);  
Email: [a.adawi@hull.ac.uk](mailto:a.adawi@hull.ac.uk)

**Jean-Sebastien G. Bouillard** – *Department of Physics and Mathematics, University of Hull, Kingston upon Hull HU6 7RX, United Kingdom;* [orcid.org/0000-0002-6942-1749](https://orcid.org/0000-0002-6942-1749); Email: [j.bouillard@hull.ac.uk](mailto:j.bouillard@hull.ac.uk)

**Mary O'Neill** – *School of Science and Technology, Nottingham Trent University, Nottingham NG11 8NS, United Kingdom;* Email: [mary.oneill@ntu.ac.uk](mailto:mary.oneill@ntu.ac.uk)

### Author

**Emanuele Verrelli** – *Department of Physics and Mathematics, University of Hull, Kingston upon Hull HU6 7RX, United Kingdom*

Complete contact information is available at: <https://pubs.acs.org/10.1021/acsomega.3c06932>

### Notes

The authors declare no competing financial interest.

## ■ ACKNOWLEDGMENTS

The authors acknowledge the Iraqi Ministry of Higher Education and Scientific Research (MOHESR) and the Department of Applied Sciences, University of Technology-Iraq for partly funding this work.

## ■ REFERENCES

- (1) Ibrahim, M. A.; Verrelli, E.; Lai, K. T.; Kyriakou, G.; Lee, A. F.; Isaacs, M. A.; Cheng, F.; O'Neill, M. Dual Wavelength (Ultraviolet and Green) Photodetectors Using Solution Processed Zinc Oxide Nanoparticles. *ACS Appl. Mater. Interfaces* **2017**, *9* (42), 36971–36979.
- (2) Banerjee, S.; Pillai, S. C.; Falaras, P.; O'Shea, K. E.; Byrne, J. A.; Dionysiou, D. D. New Insights into the Mechanism of Visible Light Photocatalysis. *J. Phys. Chem. Lett.* **2014**, *5* (15), 2543–2554.
- (3) Suwondo, K. P.; Aprilita, N. H.; Wahyuni, E. T. Enhancement of TiO<sub>2</sub> Photocatalytic Activity under Visible Light by Doping with Cu from Electroplating Wastewater. *React. Kinet., Mech. Catal.* **2022**, *135* (1), 479–497.
- (4) Ding, Y.; Ding, B.; Kanda, H.; Usiobo, O. J.; Gallet, T.; Yang, Z.; Liu, Y.; Huang, H.; Sheng, J.; Liu, C.; et al. Single-Crystalline TiO<sub>2</sub> Nanoparticles for Stable and Efficient Perovskite Modules. *Nat. Nanotechnol.* **2022**, *17* (6), 598–605.
- (5) Nunes, D.; Fortunato, E.; Martins, R. Flexible Nanostructured TiO<sub>2</sub>-Based Gas and UV Sensors: A Review. *Discovery Mater.* **2022**, *2* (1), No. 2.
- (6) Shu, J.; Qiu, Z.; Lv, S.; Zhang, K.; Tang, D. Plasmonic Enhancement Coupling with Defect-Engineered TiO<sub>2</sub>–X: A Mode for Sensitive Photoelectrochemical Biosensing. *Anal. Chem.* **2018**, *90* (4), 2425–2429.
- (7) Dharma, H. N. C.; Jaafar, J.; Widiastuti, N.; Matsuyama, H.; Rajabsadeh, S.; Othman, M. H. D.; Rahman, M. A.; Jafri, N. N. M.; Suhaimin, N. S.; Nasir, A. M.; Alias, N. H. A Review of Titanium Dioxide (TiO<sub>2</sub>)-Based Photocatalyst for Oilfield-Produced Water Treatment. *Membranes* **2022**, *12* (3), No. 345, DOI: [10.3390/membranes12030345](https://doi.org/10.3390/membranes12030345).
- (8) Xie, Y.; Wei, L.; Li, Q.; Chen, Y.; Liu, H.; Yan, S.; Jiao, J.; Liu, G.; Mei, L. A High Performance Quasi-Solid-State Self-Powered UV Photodetector Based on TiO<sub>2</sub> Nanorod Arrays. *Nanoscale* **2014**, *6* (15), 9116–9121, DOI: [10.1039/C4NR01665C](https://doi.org/10.1039/C4NR01665C).
- (9) Imran, M.; Saeed, Z.; Pervaiz, M.; Mehmood, K.; Ejaz, R.; Younas, U.; Nadeem, H. A.; Hussain, S. Enhanced Visible Light Photocatalytic Activity of TiO<sub>2</sub> Co-Doped with Fe, Co, and S for Degradation of Congo Red. *Spectrochim. Acta, Part A* **2021**, *255*, No. 119644.
- (10) Sirivallop, A.; Areerob, T.; Chiarakorn, S. Enhanced Visible Light Photocatalytic Activity of N and Ag Doped and Co-Doped TiO<sub>2</sub> Synthesized by Using an In-Situ Solvothermal Method for Gas Phase Ammonia Removal. *Catalysts* **2020**, *10* (2), No. 251, DOI: [10.3390/catal10020251](https://doi.org/10.3390/catal10020251).
- (11) Xu, Y.; Wu, S.; Wan, P.; Sun, J.; Hood, Z. D. Introducing Ti 3+ Defects Based on Lattice Distortion for Enhanced Visible Light Photoreactivity in TiO<sub>2</sub> Microspheres. *RSC Adv.* **2017**, *7* (52), 32461–32467.
- (12) Pan, L.; Wang, S.; Xie, J.; Wang, L.; Zhang, X.; Zou, J.-J. Constructing TiO<sub>2</sub> P-n Homojunction for Photoelectrochemical and

- Photocatalytic Hydrogen Generation. *Nano Energy* **2016**, *28*, 296–303.
- (13) Chen, X.; Liu, L.; Huang, F. Black Titanium Dioxide (TiO<sub>2</sub>) Nanomaterials. *Chem. Soc. Rev.* **2015**, *44* (7), 1861–1885.
- (14) Wang, B.; Kerr, L. L. Stability of CdS-Coated TiO<sub>2</sub> Solar Cells. *J. Solid State Electrochem.* **2012**, *16* (3), 1091–1097.
- (15) Ng, C.; Cadusch, J. J.; Dligatch, S.; Roberts, A.; Davis, T. J.; Mulvaney, P.; Gómez, D. E. Hot Carrier Extraction with Plasmonic Broadband Absorbers. *ACS Nano* **2016**, *10* (4), 4704–4711.
- (16) Ibrahim, M. A.; Verrelli, E.; Cheng, F.; Adawi, A. M.; Bouillard, J.-S. G.; O'Neill, M. Persistent Near-Infrared Photoconductivity of ZnO Nanoparticles Based on Plasmonic Hot Charge Carriers. *J. Appl. Phys.* **2022**, *131* (10), No. 103103.
- (17) Cushing, S. K.; Li, J.; Meng, F.; Senty, T. R.; Suri, S.; Zhi, M.; Li, M.; Bristow, A. D.; Wu, N. Photocatalytic Activity Enhanced by Plasmonic Resonant Energy Transfer from Metal to Semiconductor. *J. Am. Chem. Soc.* **2012**, *134* (36), 15033–15041.
- (18) Naldoni, A.; Allieta, M.; Santangelo, S.; Marelli, M.; Fabbri, F.; Cappelli, S.; Bianchi, C. L.; Psaro, R.; Dal Santo, V. Effect of Nature and Location of Defects on Bandgap Narrowing in Black TiO<sub>2</sub> Nanoparticles. *J. Am. Chem. Soc.* **2012**, *134* (18), 7600–7603.
- (19) Pan, X.; Xu, Y.-J. Defect-Mediated Growth of Noble-Metal (Ag, Pt, and Pd) Nanoparticles on TiO<sub>2</sub> with Oxygen Vacancies for Photocatalytic Redox Reactions under Visible Light. *J. Phys. Chem. C* **2013**, *117* (35), 17996–18005.
- (20) Chen, W.; Lu, Y.; Dong, W.; Chen, Z.; Shen, M. Plasmon Mediated Visible Light Photocurrent and Photoelectrochemical Hydrogen Generation Using Au Nanoparticles/TiO<sub>2</sub> Electrode. *Mater. Res. Bull.* **2014**, *50*, 31–35.
- (21) Li, X.; Gao, C.; Duan, H.; Lu, B.; Pan, X.; Xie, E. Nanocrystalline TiO<sub>2</sub> Film Based Photoelectrochemical Cell as Self-Powered UV-Photodetector. *Nano Energy* **2012**, *1* (4), 640–645.
- (22) Wang, Z.; Ran, S.; Liu, B.; Chen, D.; Shen, G. Multilayer TiO<sub>2</sub> Nanorod Cloth/Nanorod Array Electrode for Dye-Sensitized Solar Cells and Self-Powered UV Detectors. *Nanoscale* **2012**, *4* (11), 3350–3358, DOI: 10.1039/c2nr30440f.
- (23) Lee, W.-J.; Hon, M.-H. An Ultraviolet Photo-Detector Based on TiO<sub>2</sub> /Water Solid-Liquid Heterojunction. *Appl. Phys. Lett.* **2011**, *99* (25), No. 251102.
- (24) Cao, C.; Hu, C.; Wang, X.; Wang, S.; Tian, Y.; Zhang, H. UV Sensor Based on TiO<sub>2</sub> Nanorod Arrays on FTO Thin Film. *Sensors Actuators, B* **2011**, *156* (1), 114–119.
- (25) Chen, J.; Hu, B.; Chen, C.; Lv, X.; San, H.; Hofmann, W. In A High-Performance Self-Powered UV Photodetector Based on Self-Doping TiO<sub>2</sub> Nanotube Arrays, 2019 20th International Conference on Solid-State Sensors, Actuators and Microsystems & Eurosensors XXXIII (TRANSDUCERS & EUROSENSORS XXXIII); IEEE, 2019; pp 1329–1332.
- (26) Gao, Y.; Xu, J.; Shi, S.; Dong, H.; Cheng, Y.; Wei, C.; Zhang, X.; Yin, S.; Li, L. TiO<sub>2</sub> Nanorod Arrays Based Self-Powered UV Photodetector: Heterojunction with NiO Nanoflakes and Enhanced UV Photoresponse. *ACS Appl. Mater. Interfaces* **2018**, *10* (13), 11269–11279.
- (27) Ferhati, H.; Djeflal, F.; Martin, N. Highly Improved Responsivity of Self-Powered UV–Visible Photodetector Based on TiO<sub>2</sub>/Ag/TiO<sub>2</sub> Multilayer Deposited by GLAD Technique: Effects of Oriented Columns and Nano-Sculptured Surface. *Appl. Surf. Sci.* **2020**, *529*, No. 147069.
- (28) Chen, J.; Xu, J.; Shi, S.; Cao, R.; Liu, D.; Bu, Y.; Yang, P.; Xu, J.; Zhang, X.; Li, L. Novel Self-Powered Photodetector with Binary Photoswitching Based on SnS x /TiO<sub>2</sub> Heterojunctions. *ACS Appl. Mater. Interfaces* **2020**, *12* (20), 23145–23154.
- (29) Tan, F.; Li, T.; Wang, N.; Lai, S. K.; Tsoi, C. C.; Yu, W.; Zhang, X. Rough Gold Films as Broadband Absorbers for Plasmonic Enhancement of TiO<sub>2</sub> Photocurrent over 400–800 Nm. *Sci. Rep.* **2016**, *6*, No. 33049.
- (30) Naldoni, A.; Fabbri, F.; Altomare, M.; Marelli, M.; Psaro, R.; Sellì, E.; Salviati, G.; Dal Santo, V. The Critical Role of Intragap States in the Energy Transfer from Gold Nanoparticles to TiO<sub>2</sub>. *Phys. Chem. Chem. Phys.* **2015**, *17* (7), 4864–4869.
- (31) Xue, X.; Ji, W.; Mao, Z.; Mao, H.; Wang, Y.; Wang, X.; Ruan, W.; Zhao, B.; Lombardi, J. R. Raman Investigation of Nanosized TiO<sub>2</sub>: Effect of Crystallite Size and Quantum Confinement. *J. Phys. Chem. C* **2012**, *116* (15), 8792–8797.
- (32) Gorzkowska-Sobas, A.; Kusior, E.; Radecka, M.; Zakrzewska, K. Visible Photocurrent Response of TiO<sub>2</sub> Anode. *Surf. Sci.* **2006**, *600* (18), 3964–3970.
- (33) Chen, Z.; Zhu, Z.; Huang, L.; Cheng, C. High Sensitivity UV Photodetectors Based on Low-Cost TiO<sub>2</sub> P25-Graphene Hybrids. *Nanotechnology* **2022**, *33* (8), No. 08LT01.
- (34) Yu, Y.; Wen, W.; Qian, X. Y.; Liu, J. B.; Wu, J. M. UV and Visible Light Photocatalytic Activity of Au/TiO<sub>2</sub> Nanoforests with Anatase/Rutile Phase Junctions and Controlled Au Locations. *Sci. Rep.* **2017**, *7*, No. 41253, DOI: 10.1038/srep41253.
- (35) Luna, M.; Barawi, M.; Gómez-Moñivas, S.; Colchero, J.; Rodríguez-Peña, M.; Yang, S.; Zhao, X.; Lu, Y.-H.; Chintala, R.; Reñones, P.; et al. Photoinduced Charge Transfer and Trapping on Single Gold Metal Nanoparticles on TiO<sub>2</sub>. *ACS Appl. Mater. Interfaces* **2021**, *13* (42), 50531–50538.
- (36) Arshad, M. S.; Trafela, Š.; Rožman, K. Ž.; Kovač, J.; Djinović, P.; Pintar, A. Determination of Schottky Barrier Height and Enhanced Photoelectron Generation in Novel Plasmonic Immobilized Multi-segmented (Au/TiO<sub>2</sub>) Nanorod Arrays (NRAs) Suitable for Solar Energy Conversion Applications. *J. Mater. Chem. C* **2017**, *5* (40), 10509–10516.
- (37) Fowler, R. H. The Analysis of Photoelectric Sensitivity Curves for Clean Metals at Various Temperatures. *Phys. Rev.* **1931**, *38* (1), 45–56.
- (38) Ouyang, W.; Teng, F.; Jiang, M.; Fang, X. ZnO Film UV Photodetector with Enhanced Performance: Heterojunction with CdMoO<sub>4</sub> Microplates and the Hot Electron Injection Effect of Au Nanoparticles. *Small* **2017**, *13* (39), No. 1702177.
- (39) Lee, H.; Song, K.; Lee, M.; Park, J. Y. In Situ Visualization of Localized Surface Plasmon Resonance-Driven Hot Hole Flux. *Adv. Sci.* **2020**, *7* (20), No. 2001148.
- (40) Yan, T.; Cai, S.; Hu, Z.; Li, Z.; Fang, X. Ultrafast Speed, Dark Current Suppression, and Self-Powered Enhancement in TiO<sub>2</sub> -Based Ultraviolet Photodetectors by Organic Layers and Ag Nanowires Regulation. *J. Phys. Chem. Lett.* **2021**, *12* (40), 9912–9918.
- (41) Wu, K.; Chen, J.; McBride, J. R.; Lian, T. Efficient Hot-Electron Transfer by a Plasmon-Induced Interfacial Charge-Transfer Transition. *Science* **2015**, *349* (6248), 632–635.
- (42) Giugni, A.; Torre, B.; Toma, A.; Francardi, M.; Malerba, M.; Alabastri, A.; Zaccaria, R. P.; Stockman, M. I.; Di Fabrizio, E. Hot-Electron Nanoscopy Using Adiabatic Compression of Surface Plasmons. *Nat. Nanotechnol.* **2013**, *8* (11), 845–852, DOI: 10.1038/nnano.2013.207.
- (43) Zhang, J.; Toe, C. Y.; Kumar, P.; Scott, J.; Amal, R. Engineering Defects in TiO<sub>2</sub> for the Simultaneous Production of Hydrogen and Organic Products. *Appl. Catal., B* **2023**, *333*, No. 122765.
- (44) Nishijima, Y.; Ueno, K.; Yokota, Y.; Murakoshi, K.; Misawa, H. Plasmon-Assisted Photocurrent Generation from Visible to near-Infrared Wavelength Using a Au-Nanorods/TiO<sub>2</sub> Electrode. *J. Phys. Chem. Lett.* **2010**, *1* (13), 2031–2036.
- (45) Shi, X.; Kosei, U.; Naoki, T.; Hiroaki, M. Plasmon-Enhanced Photocurrent Generation and Water Oxidation with a Gold Nanoisland-Loaded Titanium Dioxide Photoelectrode. *J. Phys. Chem. C* **2013**, *117*, 2494–2499.
- (46) Kumbhar, S. M.; Shevate, S. S.; Patil, A. R.; Shaikh, S. K.; Rajpure, K. Y. Dip Coated TiO<sub>2</sub> Based Metal-Semiconductor-Metal Ultraviolet Photodetector for UV A Monitoring. *Superlattices Microstruct.* **2020**, *141*, No. 106490.
- (47) Joshna, P.; Hazra, A.; Chappanda, K. N.; Pattnaik, P. K.; Kundu, S. Fast Response of UV Photodetector Based on Ag Nanoparticles Embedded Uniform TiO<sub>2</sub> Nanotubes Array. *Semicond. Sci. Technol.* **2020**, *35* (1), No. 015001.

- (48) Gao, X. D.; Fei, G. T.; Xu, S. H.; Zhong, B. N.; Ouyang, H. M.; Li, X. H.; Zhang, L. De. Porous Ag/TiO<sub>2</sub>-Schottky-Diode Based Plasmonic Hot-Electron Photodetector with High Detectivity and Fast Response. *Nanophotonics* **2019**, *8* (7), 1247–1254.
- (49) Ghosh, C.; Dwivedi, S. M. M. D.; Ghosh, A.; Dalal, A.; Mondal, A. A Novel Ag Nanoparticles/TiO<sub>2</sub> Nanowires-Based Photodetector and Glucose Concentration Detection. *Appl. Phys. A* **2019**, *125* (12), No. 810, DOI: 10.1007/s00339-019-3108-5.
- (50) Xie, Y.; Wei, L.; Li, Q.; Wei, G.; Wang, D.; Chen, Y.; Jiao, J.; Yan, S.; Liu, G.; Mei, L. Self-Powered Solid-State Photodetector Based on TiO<sub>2</sub> Nanorod/Spiro-MeOTAD Heterojunction. *Appl. Phys. Lett.* **2013**, *103* (26), No. 261109, DOI: 10.1063/1.4858390.
- (51) Das Mahapatra, A.; Das, A.; Ghosh, S.; Basak, D. Defect-Assisted Broad-Band Photosensitivity with High Responsivity in Au/Self-Seeded TiO<sub>2</sub> NR/Au-Based Back-to-Back Schottky Junctions. *ACS Omega* **2019**, *4* (1), 1364–1374.
- (52) Pescaglioni, A.; Martín, A.; Cammi, D.; Juska, G.; Ronning, C.; Pelucchi, E.; Iacopino, D. Hot-Electron Injection in Au Nanorod–ZnO Nanowire Hybrid Device for Near-Infrared Photodetection. *Nano Lett.* **2014**, *14* (11), 6202–6209, DOI: 10.1021/nl5024854.
- (53) Wang, W.; Klots, A.; Prasai, D.; Yang, Y.; Bolotin, K. L.; Valentine, J. Hot Electron-Based Near-Infrared Photodetection Using Bilayer MoS<sub>2</sub>. Yang, Kirill I. Bolotin, and Jason Valentine. *Nano Lett.* **2015**, *15* (11), 7440–7444, DOI: 10.1021/acs.nanolett.5b02866.
- (54) Sessolo, M.; Bolink, H. J. Hybrid Organic-Inorganic Light-Emitting Diodes. *Adv. Mater.* **2011**, *23* (16), 1829–1845.
- (55) Jin, Y.; Wang, J.; Sun, B.; Blakesley, J. C.; Greenham, N. C. Solution-Processed Ultraviolet Photodetectors Based on Colloidal ZnO Nanoparticles. *Nano Lett.* **2008**, *8* (6), 1649–1653.
- (56) Ibrahim, M. A.; Rasheed, B. G.; Mahdi, R. I.; Khazal, T. M.; Omar, M. M.; O'Neill, M. Plasmonic-Enhanced Photocatalysis Reactions Using Gold Nanostructured Films. *RSC Adv.* **2020**, *10* (38), 22324–22330.
- (57) Li, J.; Cushing, S. K.; Meng, F.; Senty, T. R.; Bristow, A. D.; Wu, N. Plasmon-Induced Resonance Energy Transfer for Solar Energy Conversion. *Nat. Photonics* **2015**, *9* (9), 601–607.
- (58) Georgakopoulos, T.; Todorova, N.; Karapati, S.; Pomoni, K.; Trapalis, C. Photoconductivity Studies on Surface Modified TiO<sub>2</sub> Nanoparticles. *Mater. Sci. Semicond. Process.* **2019**, *99*, 175–181.
- (59) Majumder, S.; Jana, S. K.; Bagani, K.; Satpati, B.; Kumar, S.; Banerjee, S. Fluorescence Resonance Energy Transfer and Surface Plasmon Resonance Induced Enhanced Photoluminescence and Photoconductivity Property of Au–TiO<sub>2</sub>Metal–Semiconductor Nanocomposite. *Opt. Mater.* **2015**, *40*, 97–101.
- (60) Wang, W.; Zhang, C.; Qiu, K.; Li, G.; Zhai, A.; Hao, Y.; Li, X.; Cui, Y. Enhancing Hot-Electron Photodetection of a TiO<sub>2</sub>/Au Schottky Junction by Employing a Hybrid Plasmonic Nanostructure. *Materials* **2022**, *15* (8), No. 2737, DOI: 10.3390/ma15082737.
- (61) Noothongkaew, S.; Han, J. K.; Lee, Y. B.; Thumthan, O.; An, K.-S. Au NPs Decorated TiO<sub>2</sub> Nanotubes Array Candidate for UV Photodetectors. *Prog. Nat. Sci.: Mater. Int.* **2017**, *27* (6), 641–646.
- (62) Zhang, Y.; Zhou, R.; Xu, R.; Fang, L.; Zhou, J.; Chen, Y.; Ruan, S. Visible-Blind Self-Powered Ultraviolet Photodetector Based on CuI/TiO<sub>2</sub> Nanostructured Heterojunctions. *ACS Appl. Nano Mater.* **2022**, *5* (11), 16804–16811.
- (63) Schneider, J.; Matsuoka, M.; Takeuchi, M.; Zhang, J.; Horiuchi, Y.; Anpo, M.; Bahnemann, D. W. Understanding TiO<sub>2</sub> photocatalysis: Mechanisms and Materials. *Chem. Rev.* **2014**, *114* (19), 9919–9986.
- (64) Zhang, X.; Chen, Y. L.; Liu, R. S.; Tsai, D. P. Plasmonic Photocatalysis. *Rep. Prog. Phys.* **2013**, *76* (4), No. 046401.